SYNERGY OF TECTONIC GEOMORPHOLOGY, APPLIED GEOPHYSICS AND REMOTE SENSING TECHNIQUES REVEALS NEW DATA FOR ACTIVE EXTENSIONAL TECTONISM IN NW PELOPONNESE (GREECE)

AUTHORS

Fountoulis Ioannis[†], Vassilakis Emmanuel[1*], Mavroulis Spyridon[2], Alexopoulos John[3], Dilalos Spyridon[3], Erkeki Athanasia[4]

[1*] National and Kapodistrian University of Athens, Faculty of Geology and Geoenvironment, Department of Geography & Climatology, Panepistimiopolis Zografou, 15784 (corresponding author)

[2] National and Kapodistrian University of Athens, Faculty of Geology and Geoenvironment, Department of Dynamic Tectonic Applied Geology, Panepistimiopolis Zografou, 15784

[3] National and Kapodistrian University of Athens, Faculty of Geology and Geoenvironment, Department of Geophysics-Geothermy, Panepistimiopolis Zografou, 15784

[4] National and Kapodistrian University of Athens, Faculty of Geology and Geoenvironment, Laboratory of Natural Hazards' Prevention & Management, Panepistimiopolis Zografou, 15784

ABSTRACT

In tectonically active areas like NW Peloponnese (W. Greece) the morphogenetic processes are strongly influenced by the activity of faults, which in many cases cannot be easily traced. In this paper a multidisciplinary analysis (morphometric indices, neotectonic mapping, geophysical surveys and remote sensing techniques) is applied aiming to map the unknown (until recently) E-W trending Pineios River normal fault zone with high accuracy and understand its implications to the evolution of the very significant ancient territory of Elis, during Holocene. Its activity seem to reflect on the river flow path frequent changes as well as the nearby shoreline displacements, since we argue that this is the main reason for the migration of Pineios river mouth for several times during the historical times.

The quantification of deformation caused by the fault activity was studied through the application of proposed morphotectonic indices such as drainage network asymmetry, sinuosity, as well as mountain front sinuosity yielding that this is a definitely active structure. High slip rates were calculated reaching the value of 0.48 mm/yr for the last 209 ky (based on already published dating) whilst this was also verified by applied geophysical methodologies. The fault surface discontinuity was identified in depth by using vertical electrical resistivity measurements, since the deposited layers of different resistivity behavior were found clearly interrupted. The layer displacement increases towards west, reaching the value of 110 meters. The most spectacular landform alteration due to this surface deformation is the migration of the river estuary from north to south and vice versa, at completely different open sea areas, during Upper Quaternary and mostly in Holocene. The sediment transportation path has been altered several times after these significant changes and the most recent seem to have happened almost 2,000 years ago. The river estuary finally migrated to its contemporary location at the southern coast -settled on the hanging wall- inducing retrograding of the northern coast -settled on the foot wall- with rates reaching the order of 0.52 m/yr, as this was induced by the interpretation of historical and recently acquired remote sensing data.

KEYWORDS

morphotectonic indices, fault slip rate, photogrammetry, digital shoreline analysis, vertical electrical sounding

1 INTRODUCTION

NW Peloponnese is located at the external part of the Hellenic Orogenic Arc, just a few tens of kilometers internally from the Hellenic Trench and has been repeatedly suffered damages by large seismic events and earthquake related geo-environmental phenomena until very recently (June 8th 2008, Mw=6.4) (Lekkas et al., 2008; Konstantinou et al., 2009; Feng et al., 2010; Koukouvelas et al., 2010; Mavroulis et al., 2010; Margaris et al., 2010; Papadopoulos et al., 2010; Mavroulis et al., 2013). The recorded seismic activity at this region is continuous during the entire historical period (Papazachos and Papazachou, 1997) and thus it is important to understand the slip behavior of faults that have already caused or may cause earthquakes in the near future. Pineios fault zone is a tectonic structure that has never been mapped till very recently, as it has never been assigned to any historical earthquake (Mavroulis, 2009). It is located at NW Peloponnese and has drastically affected the Lower Pineios River plain, along which Ancient Elis was developed during the Hellenistic and Roman periods (Kraft et al., 2005).

Today, the ruins of Ancient Elis are lying downstream of the modern Pineios artificial dam and its abandonment seems to have been caused by several geodynamic processes, which might be related to the active tectonism of the wider region (Guidoboni et al., 1994). We argue in this paper that the fault activity caused the river estuary relocation and consequently secondary landform processing phenomena have been developed throughout the Pineios downstream broader area during Upper Quaternary (Fountoulis et al., 2011; 2013). The combination of methodologies described in this paper includes tectonic geomorphology analysis, applied geophysics measurements and remote sensing techniques and aims to (a) assess the tectonic activity of Pineios fault zone, (b) provide quantitative information for the degree of the fault activity, (c) clarify the stratigraphic sequence of the layered geological formations underlying the study area, (d) accurately map the fault zone in depth and estimate its displacement, (e) quantify the influence of the active faulting to the coastal environment.

2 GEOLOGICAL SETTING

The westernmost part of Peloponnese that is described in this paper is an area with generally low relief (Fig.1) and mostly covered by recently deposited sediments (Kamberis et al., 1993). The post-alpine sequences that have been observed throughout the Pyrgos-Olympia basin are of Pliocene and Quaternary age and lie unconformably on the alpine basement. Their geographical distribution and variety of facies (marine, lagoonal, lacustrine and terrestrial) clearly reflect vertical fault block movements during the neotectonic period and ongoing active tectonism (Lekkas et al., 1992). According to already published geological mapping data (Kamberis et al., 1993) and paleontological findings and analyses (Athanassiou, 2000), as well as $^{230}Th/^{238}U$ dating of corals found in the marine terraces of NW Peloponnese (Stamatopulos et al., 1988), a typical stratigraphic section for the post-alpine succession may be constructed representing the paleo-environment changes after Pliocene. More specifically the sediment sequence consists of: (a) lacustrine and lagoonal marls of Upper Pliocene – Pleistocene, (b) shallow marine sands, sandstones and conglomerates of Pleistocene, (c) marine calcareous sandstones of Pleistocene, and (d) Holocene alluvial deposits (sands, gravels) of the Lower Pineios River valley that unconformably overlain the above mentioned formations. The Plio-Pleistocene molluscan assemblages and the sedimentary facies imply a continuous alternation of shallow marine waters, brackish and lacustrine environments (Paraskevaidis and Symeonidis, 1965). The broader region of Pineios valley is already known for the existence of fossil Mammals, as some Hippopotamus (Thenius, 1955, Symeonidis and Therodorou, 1986) and Elephas (Kamberis, 1987, Athanassiou, 2000) specimens have been discovered, indicating a pre-existing fluvial-lacustrine environment. Kamberis et al. (1993) based on deep borehole data proved that the maximum thickness of this post-alpine sequence exceeds 3,000 meters and unconformably covers the basement rock pile.

The alpine basement comprises of three alpine geotectonic units; thin bedded pelagic sediments of Pindos unit are found overthrusting neritic carbonates and flysch of Gavrovo-Tripolis unit, which are also overthrusting evaporites, limestones and flysch of the most external Ionian unit (Papanikolaou, 1984; 1997).

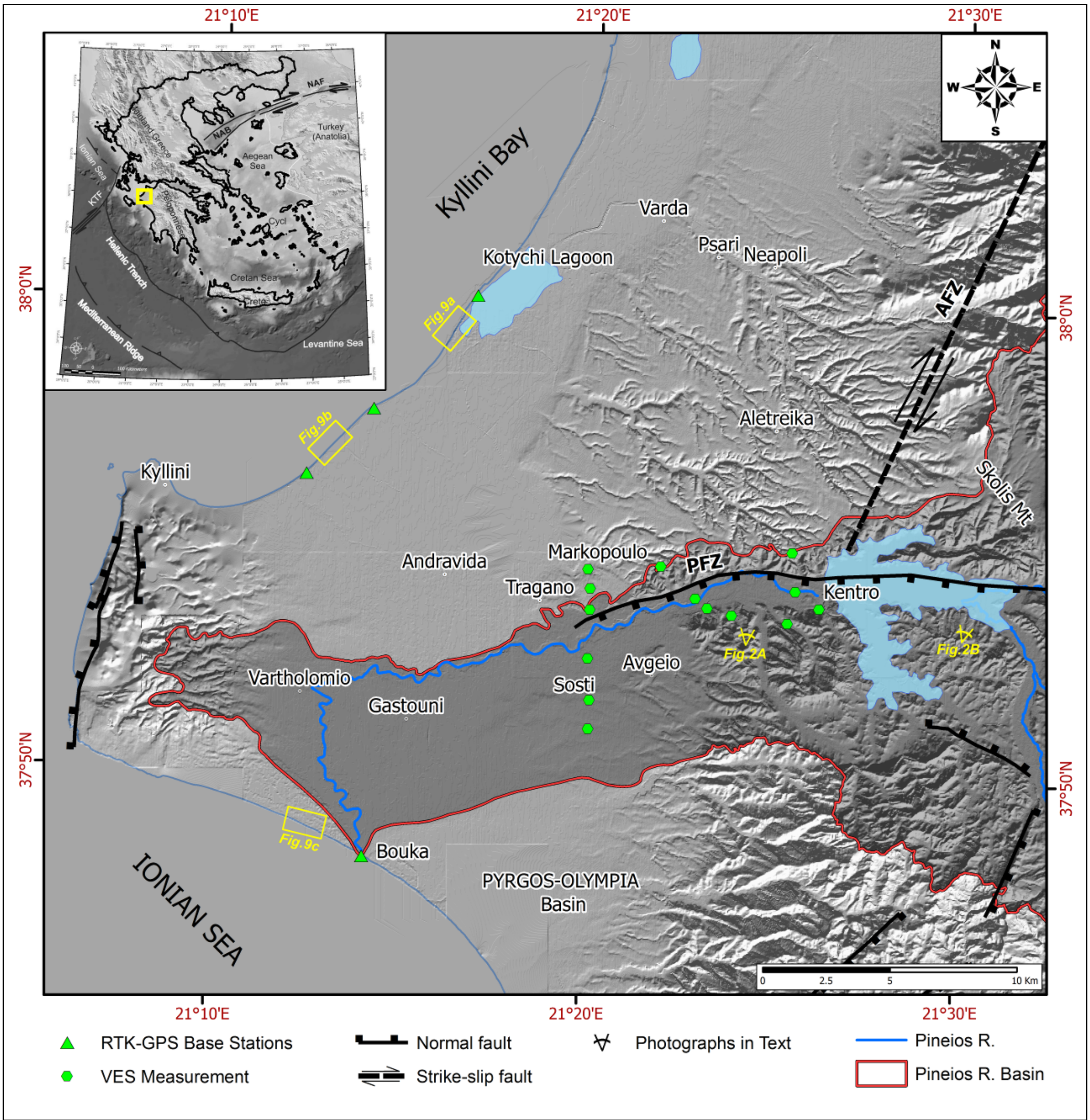

Figure 1. Index map of the study area at NW Peloponnese. The trace of the studied active fault is illustrated just north of Pineios River. This structure is responsible for a number of landform processes which are described in the text.

2.1 Regional active tectonics

The Ionian Islands and the Gulf of Corinth are included in the most seismic and tectonically active regions in Greece (Hatzfeld et al., 1990). NW Peloponnese is the geotectonic junction connecting those rapidly evolving areas (Vassilakis et al., 2011). The intense tectonic activity is continuous from Miocene till Holocene (Hollenstein et al., 2006 and references therein) due to its placement at the external part of the Hellenic orogenic forearc and its proximity to the present day NNW-SSE trending Hellenic Trench that represents the active subduction boundary between the African and the European plates. Additionally, the ongoing diapirism of the Triassic evaporites of the Ionian unit alpine basement is a process which amplifies the geotectonic instability in a non-systematic way (Underhill, 1988).

Several active faults have been mapped and studied during neotectonic surveys; some of these were active in previous periods (e.g., Pliocene, Pleistocene) whereas a number of them are still active since Holocene (Mariolakos et al., 1991, Lekkas et al., 1992). The recorded seismicity level, which is possibly one of the highest in the Mediterranean region (Hatzfeld et al., 1990), confirms the neotectonic studies, which show that the broader area is undergoing intense tectonic deformation. According to historical and instrumental records, numerous destructive earthquakes have taken place in the area since 399 BC, most of which -if not all- were shallow (<20 km) and have been assigned to high intensities (Papazachos and Papazachou, 1997).

The neotectonic structure of NW Peloponnese is characterized by large and independently moving neotectonic blocks that form grabens and horsts bounded by fault zones, which are either visible or concealed. These extensional structures trend mainly E-W or NNW-SSE and create a complex matrix of neotectonic blocks with particular evolution characteristics and relative displacements (Mariolakos et al., 1985). The sedimentation processes were highly influenced by the dominant neotectonic regime that is active throughout the deposition imprinted in syn-sedimentary formations (Papanikolaou et al., 2007).

The main neotectonic macrostructure of the study area is the Pyrgos – Olympia post-alpine basin, which covers an area of 1500 km^2. The marginal fault zones are clearly discernible and form impressive morphological discontinuities (Lekkas et al., 1992; 2000; Fountoulis et al, 2007). The basin itself is infilled with post-alpine deposits of Late Miocene – Holocene age, reaching a thickness of approximately 3km (Kamberis, 1987).

The Pineios normal fault zone trace is observed SSW of Skolis Mt and was not identified until very recently (Mavroulis, 2009). It is a generally E-W trending structure, dipping southwards. Its surficial expression coincides with a slightly degraded but clearly observable morphological discontinuity extending eastwards from the northernmost banks of Pineios artificial lake and westwards to Tragano village (Fig. 2). The footwall consists of post-alpine formations of Upper Pliocene - Pleistocene age overlaying unconformably the paleo-relief developed on the alpine basement. The hanging wall consists of the aforementioned post-alpine formations partially covered by the Pineios River alluvial deposits.

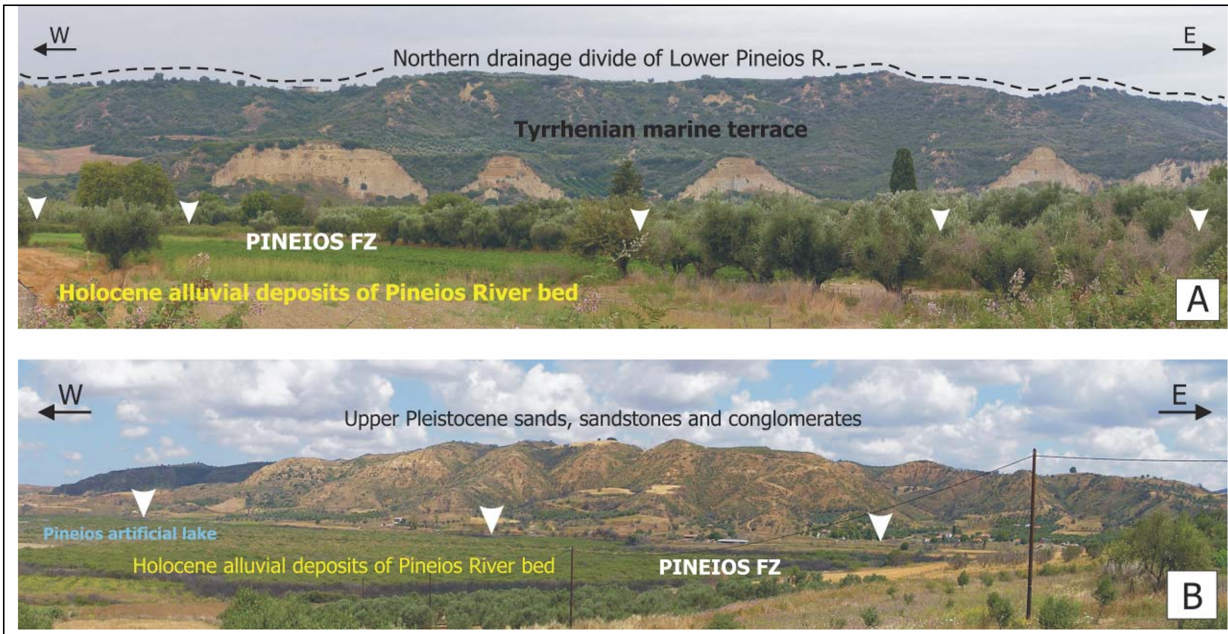

Figure 2. (A) Partial view of the area downstream of the artificial dam towards the Pineios fault zone (Pineios FZ). In this segment the footwall consists of Tyrrhenian marine terrace sediments, whilst the hanging wall is covered by Holocene alluvial deposits of Pineios riverbed. (B) Partial view of the area upstream of the artificial dam towards the Pineios fault zone (Pineios FZ). Well-preserved triangular facets are developed on Upper Pleistocene deposits. At both photographs the white arrowheads point at the fault trace.

It is worth mentioning that the post-alpine formations of the footwall form a broad Tyrrhenian marine terrace consisting of sands, sandstones and conglomerates, which outcrop both northward and southward of the fault zone for hundreds of square kilometers (Stamatopulos et al., 1988). The terraced surface appears as a monocline dipping northwestwards based on the orientation of strata according to strike and dip measurements during general geological fieldwork (Mavroulis, 2009; Mavroulis et al., 2010). More specifically, the Pleistocene marine formations of the footwall dip northwestwards at between 4° and 14° whilst the Upper Pliocene-Pleistocene marine and lagoonal formations cropping out at the hanging wall dip also northwestwards at between 7° and 30°. These fossiliferous marine deposits can often be found under a thin cover of reddish sandy and conglomeratic alluvial deposits.

Field work at the Lower Pineios River broader area has revealed enough geomorphic evidence of recent tectonic activity (Mavroulis, 2009; Mavroulis et al., 2010; Fountoulis et al., 2011; 2013; this study). The most characteristic diagnostic tectonic landforms associated with Pineios fault zone are the successive sets of slightly degraded but well-defined and well-preserved triangular facets along the morphological discontinuity formed by the displacement along the fault zone (Fig. 2). These tectonic landforms indicate active faulting and normal displacement (Wallace, 1977; Menges, 1990). They reflect rapid, recent and cumulative uplift, as only such movements can maintain these kinds of tectonic signatures in a landscape underlain by the lithologies cropping out at this region (porous marine calcareous sandstones, marine sands, sandstones, and conglomerates, lacustrine and lagoonal clays). The formation and preservation of such landforms are consistent with rapid recent uplift, which generally lasts from 10^3 to 10^6 years (Cotton, 1950; Bull, 1978). Therefore, it is rather clear that high extensional tectonic activity should be present along this mountain front and consequently the process of forming the triangular facets is quite recent.

It is worth mentioning that there was no indication of triggering any ruptures along the Pineios fault system trace after the damaging earthquake of June 2008 (Feng et al., 2010; Koukouvelas et al., 2010; Konstantinou et al., 2011). On the contrary, a significant number of rock falls were observed along the triangular facets presented here at Figure 2A, as well as liquefactions were found after the seismic event around the artificial lake (Mavroulis et al., 2013).

3 MORPHOTECTONIC ANALYSIS OF PINEIOS FAULT ZONE USING MORPHOMETRIC INDICES

Bull and McFadden (1977) introduced the approach of quantitative analysis of the topography for the evaluation of active faulting. The use of simple ratios serves as a valuable tool for tectonic geomorphology studies along faulted mountain fronts including landform metrics such as mountain–piedmont junction sinuosity, percentage of triangular faceting along mountain fronts, longitudinal river profile analyses and variations of valley floor slopes.

3.1 Mountain – Front Sinuosity (S_{mf})

Mountain front sinuosity (S_{mf}) is an index of the degree of irregularity or sinuosity along the base of a topographic escarpment. The utility of this parameter is based on the tendency of active structures to maintain straight or curvilinear profiles in map view, as contrasted to the more irregular profiles produced by erosional processes along the base of associated topographic escarpments. Mountain – front sinuosity (S_{mf}) is defined as the ratio of the observed length along the margin of the topographic mountain-piedmont junction (L_{mf}) to the overall length of the mountain front (L_s) and is given by the following equation: $S_{mf} = L_{mf} / L_s$ (Bull and McFadden, 1977; Bull, 1978). This index has already been applied in various geologic environments in active regions throughout the world revealing that the most tectonically active fronts are characterized by values of S_{mf} ranging from 1.0 to 1.4 (Bull and McFadden, 1977; Rockwell et al., 1984; Wells et al., 1988; Theocharis and Fountoulis, 2002; Silva et al., 2003). As pointed out by Wells et al. (1988), this value of S_{mf}=1.4 seems to limit the sensitivity of this index for the discrimination of any smaller-scale variation of differential uplift that may exist among different mountain fronts. Increasingly larger values of S_{mf} index (>3) are normally related to fronts with decreasing amounts of tectonic uplift relative to basal erosion or pedimentation in which the initial range – front fault may be more than 1 km away from the present erosional front (Bull and McFadden, 1977).

The S_{mf} values depend among others on topography scale. Small-scale topographic maps produce only a rough estimate of mountain front sinuosity. Therefore, mountain front sinuosity and all morphometric variables for this study were measured on large-scale topographic maps (1:5,000, with 4m contour intervals) published by the Hellenic Military Geographical Agency (HMGA).

Mountain front sinuosity was measured in three segments of the morphological discontinuity just north of Pineios valley, downstream of the artificial lake and their distinction was based on the hill-front general direction (Fig. 3). The L_{mf}, L_s and S_{mf} values for these segments are presented in table 1 whilst the S_{mf} values are also depicted in figure 3A. The calculated S_{mf} values range from 1.23 to 1.32 and according to classifications proposed by Bull and McFadden (1977), Rockwell et al. (1984), Wells et al. (1988) and Silva et al. (2003) the hill front formed by the Pineios fault zone is classified as an active one.

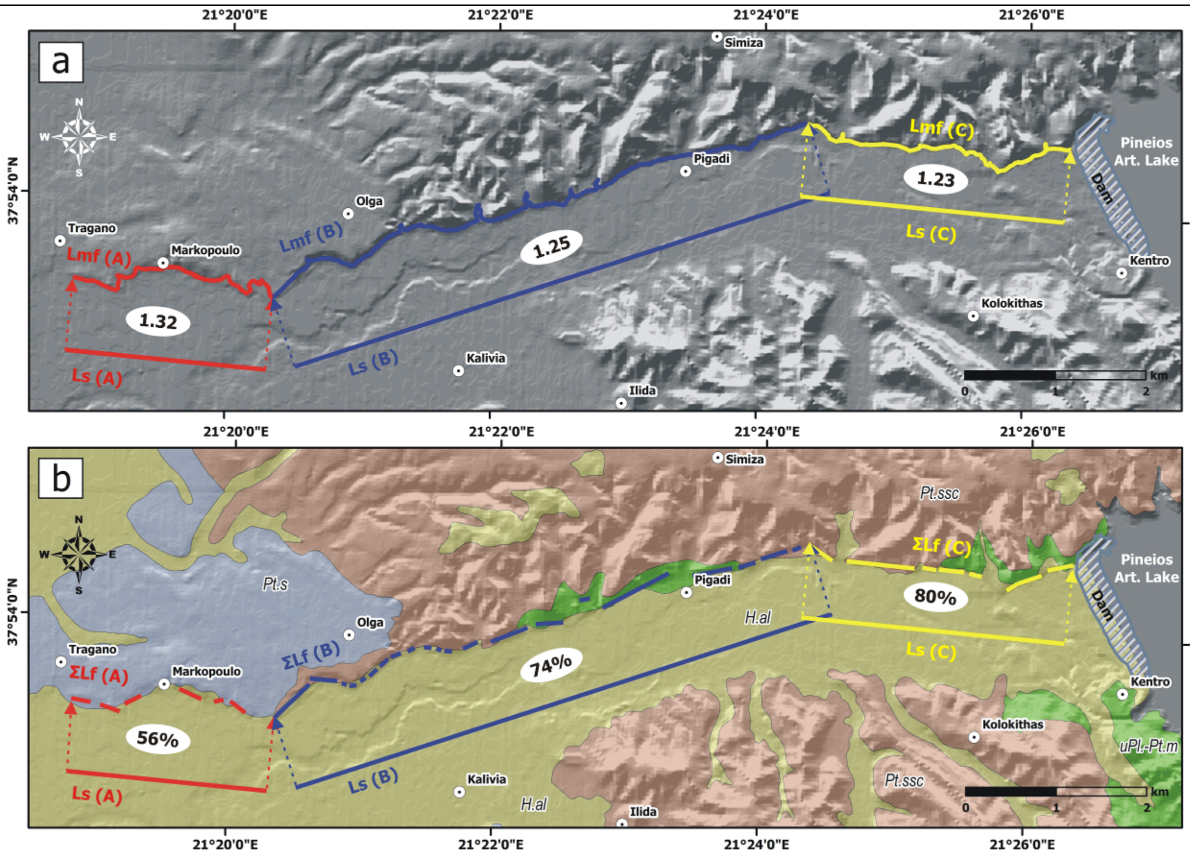

Figure 3. (a) The mountain front sinuosity (S_{mf}) values for the three segments of the morphological discontinuity north of Pineios valley are shown in the white ellipses and range from 1.23 to 1.32. According to the classifications proposed by Bull and McFadden (1977), Rockwell et al. (1984), Wells et al. (1988), Silva et al. (2003), Pineios fault zone is classified as an active tectonic structure. (b) The high percentage values (56-80%) of faceting (F%) are clear indicators for the fault activity. (H.al: Holocene deposits, Pt.s: Pleistocene calcareous sandstones, Pt.ssc: Pleistocene sands, sandstones and conglomerates, uPl.-Pt.m: Upper Pliocene-Pleistocene marls.

3.2 Percentage of faceting along mountain front (F%)

The index related to facet development and used in this study is the facet (%) index (Bull, 1978). The facet (%) index is the percentage of a given mountain front with well-shaped triangular facets and is defined as the ratio of cumulative lengths of facets (L_f) to the length of the selected mountain front

(L_s) (Wells et al., 1988). High percentages of faceting along the mountain front indicate its activity (Ramírez-Herrera, 1998). The potential difficulties on the application of this morphometric index are the systematic definition of individual facet as well as the discrimination between faceted and non-faceted sections of a mountain front (DePolo and Anderson, 2000). To avoid these difficulties and limitations, topographic maps of 1:5,000 published by the HMGA were also used.

Percentages of faceting along mountain front (F%) were measured in the above-mentioned three segments of the morphological discontinuity developed north of Pineios valley (see chapter 3.1). The measured L_f, L_s and F% calculated values for each segment are presented in table 1 and the faceting percentages are also depicted in figure 3B. The F% values range from 56% to 80% yielding high participation rates of well-defined triangular facets along the hill front of Pineios fault zone and indicating its tectonic activity.

Table 1: Mountain - front sinuosity (Smf) and percentage of faceting along the hill front (F%) for Pineios fault zone. Segments A, B, C are depicted in fig. 3.

Pineios FZ Segments	Lmf (in m)	Ls (in m)	Smf	ΣLf (in m)	Ls (in m)	F	F%
A	2926.97	2215.92	**1.32**	1230.89	2215.92	0.56	**56**
B	7738.86	6202.62	**1.25**	4598.71	6202.62	0.74	**74**
C	3595.13	2921.51	**1.23**	2340,74	2921.51	0.80	**80**

3.3 The alluvial river response to Pineios fault zone

3.3.1 Asymmetry of the Lower Pineios River network

The river valley flows adjacent to the main Pineios fault zone following an E-W direction, across the Pliocene and Pleistocene formations. The activity of Pineios fault zone seems to have caused differential vertical motion of several fault blocks accompanied by tilting in a cross-valley direction. The tilting of the fault blocks and northward migration of the Lower Pineios River valley has caused in turn the asymmetry of the drainage network developed on the hanging wall. Thus, the river shifts gradually northwards and flows adjacent and parallel to the northern drainage divide (Fig. 2). This asymmetrical development is clearly reflected on the number, size and order of the tributaries and sub basins on either side of the river. North of the 7th order Lower Pineios River, the 1st and 2nd order drainage basins prevail, while higher order drainage basins are less common and significantly smaller (Fig. 4A). In contradiction, the 3rd order drainage basins are much bigger and prevail covering an extended area at the left of the main branch of the river downstream the artificial lake. This type of asymmetric development of sub-basins yields block rotational tectonism (Cox, 1994; Garrote et al., 2006) and is in full agreement with the observations during fieldwork (Mavroulis, 2009).

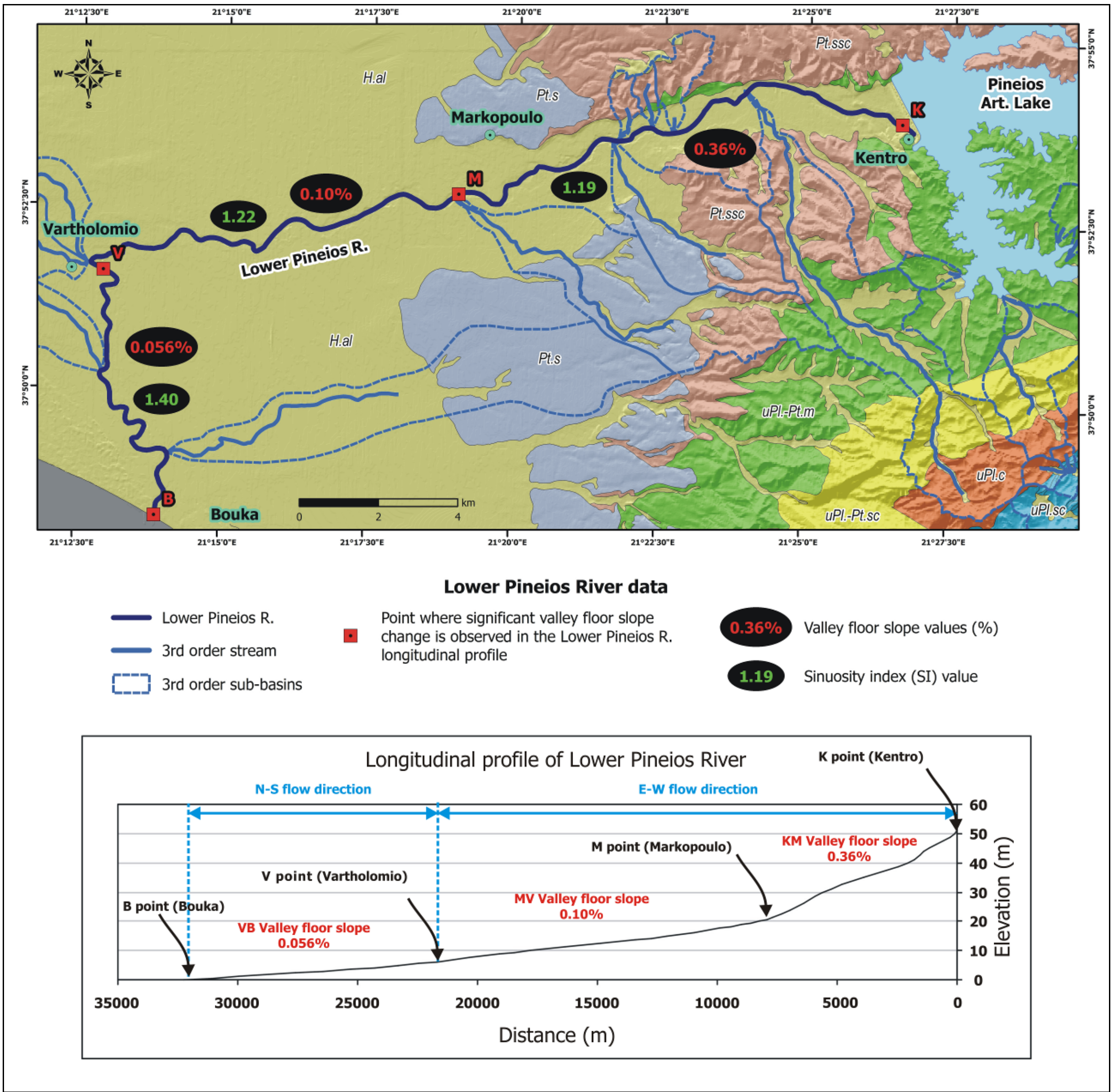

Figure 4. Significant changes are observed at the Valley Floor Slope (%) and Sinuosity Index (SI) values

after the analysis of the longitudinal profile of Lower Pineios River. The 3rd order drainage basins prevail covering an extended area south of the 7th order Lower Pineios River, while they are less common north of the main branch of the river. (H.al: Holocene deposits, Pt.s: Pleistocene calcareous sandstones, Pt.ssc: Pleistocene sands, sandstones and conglomerates, u.Pl.-Pt.m: Upper Pliocene - Pleistocene marls, u.Pl.-Pt.sc: Upper Pliocene - Pleistocene sands and clays, u.Pl.c: Upper Pliocene conglomerates, u.Pl.sc: Upper Pliocene sands and conglomerates).

3.3.2 Longitudinal profile of Lower (alluvial) Pineios River and valley floor slope changes

The information about the longitudinal profile of the Lower Pineios River from Kentro area (upstream) to Bouka area (downstream, at the contemporary river mouth) was obtained from a high resolution (2-meter) Digital Elevation Model (DEM), which was constructed after photogrammetric processing of available aerial photographs. It was segmented into three separate parts, which are (a) the upstream, (b) the intermediate and the (c) downstream segment respectively (Fig. 4). The upstream (from point K to point M) segment of the profile corresponds to the E-W trending part of the Lower Pineios River, extending from Kentro area (upstream) to Markopoulo westwards (downstream). The valley floor slope of the upstream segment was calculated at 0.36 %. The intermediate (from point M to point V) segment of the profile corresponds to the E-W trending part of the Lower Pineios River, extending from Markopoulo (upstream) to Vartholomio area westwards (downstream). The valley floor slope of the intermediate segment was calculated at 0.10 %. The downstream (from point V to point B) segment corresponds to the N-S trending and gently sloping lower course of the Lower Pineios River, extending from Vartholomio area (upstream) to Bouka area southwards (Pineios River mouth). The valley floor slope of the downstream segment was calculated at 0.056 %.

The observed valley floor slope of the upstream segment of the longitudinal profile (0.36 %) is much higher than the ones calculated for the intermediate and the downstream segments. More precisely, the average valley floor slope (0.36 %) of the upstream segment is almost 4-fold higher than the one calculated for the intermediate segment (0.10 %) and almost 6-fold higher than the one calculated for the downstream one (0.056 %). Furthermore, the valley floor slope of the intermediate segment (0.10 %) is 2-fold higher than the one calculated for the downstream segment. Based on the observation of the longitudinal profile (Fig. 4) it can be noted that the M point, where the first significant change of the valley floor slope is situated, is located in close vicinity to the westernmost edge of the morphological discontinuity. The V point, where the second significant change of the valley floor slope is situated, is located very close to Vartholomio area, where the characteristic southwards bending of the Lower Pineios River course is located. This bending seems to have tectonic origin, since it is located at the possible westwards prolongation of the Pineios fault zone, and/or due to diapiric phenomena, as the river valley seems to be diverted by the uplifted Kyllini peninsula, which is on top of an evaporitic dome (Kamberis, 1987) and bounds the Gastouni graben. It is rather clear that the subsurface tectonic deformation of the area has been imprinted at the longitudinal profile and the points where the profile anomalies were observed are the key areas for extracting conclusions about the area's neotectonic evolution.

3.3.3 Sinuosity index (SI)

Under certain conditions, alluvial rivers tend to evolve as single meandering channels (Brice, 1964; Rust, 1978). This behavior is generally influenced by tectonic movements, reflected in river channel parameters (Zámolyi et al., 2010). It is generally accepted that if a normal fault is down throwing in the downstream direction, increased meandering is resulted (Ouchi, 1985; Keller and Pinter, 1996; Holbrook and Schumm, 1999; Bridge, 2005). This process is largely independent of the river size, once the fluvial system enters the meandering stage. In this way, not only large rivers are suitable for analysis, but smaller creeks and reaches can also be evaluated, as far as they are essentially free of human influence. The increasingly use of Geographic Information Systems (GIS) and the higher quality of elevation data give the opportunity to make river sinuosity calculations a sensitive tool for recognizing neotectonic activity in low-relief areas, as even the smallest changes in the topography affect the sinuosity of low gradient rivers (Holbrook and Schumm, 1999), providing hints for points of on-going microtopographic changes. A quantitative measure of the variation of the meandering pattern is the classic sinuosity index (SI). The sinuosity index of modern river channels was defined by Leopold and Wolman (1957) as the ratio of the thalweg length to the valley length. Brice (1964) suggested a slightly modified sinuosity index (the ratio of the channel length to the length of the meander-belt axis), which has the advantage of allowing for both straight and sinuous meander-belts. In both studies, an arbitrary value of 1.5 was used to distinguish between low- and high-sinuosity channels. Although other classification schemes have been described (Schumm 1963), this value is generally accepted.

The SI values for the Lower Pineios River have been calculated using the high resolution DEM derived from aerial photographs photogrammetric processing. The calculations were made in close vicinity of the northern and western tectonic boundaries of the Gastouni graben, which are formed by the active Pineios fault zone and the Kyllini hill. This is the exact same area where the Lower Pineios River flows and especially along the three segments (see 3.3.2) characterized by different valley floor slope values derived from the longitudinal profile processing of Lower Pineios described earlier in this paper.

The sinuosity index values as well as the values of the channel length (S - curvilinear distance measurement along the center of the channel) and the valley length (L - horizontal distance measured in the thalweg of two cross sections in a linear depression between two adjacent uplands) are presented in table 2.

From upstream (KM part of the profile) to downstream (VB part of the profile), the Lower Pineios River valley floor slope decreases from 0.36 % to 0.056 %, whilst the sinuosity index values increase from 1.19 to 1.40. It is reasonable to assume that sinuosity variations along the Lower Pineios River are related to, or strongly coupled with differential tectonic deformation of the study area (differential uplift/subsidence pattern) and this is in full agreement with the thickness and the isobaths of the Neogene and Quaternary formations (Kamberis, 1987). Thus, the Lower Pineios River responds to active faulting by changing its sinuosity (Fig. 4).

Table 2: Sinuosity index (SI) and valley floor slope values calculated for Lower Pineios River. Parts KM, MV, VB are depicted in fig. 4.

Lower Pineios River part	S (in m)	L (in m)	SI	Valley floor slope (%)
KM	13154	11354	1.19	0.36
MV	11206	9175	1.22	0.10
VB	8930	6340	1.40	0.056

4 UPLIFT RATES OF FAULT BLOCKS AND PINEIOS FAULT SLIP RATE

As previously mentioned, the study area consists mainly of a succession of sediments with ages from Pliocene to Holocene. The ^{230}Th/^{238}U dating of corals (Stamatopulos et al., 1988) found in the upper layers of the sequence indicate Tyrrhenian age for all the sampled layers at three complete sections located on the footwall of Pineios fault zone. The deposition ages were determined as follows: 103 ky for Psari section (at an elevation of 40-45 m above sea level (a.s.l.)), 118 ky for Neapolis section (at an elevation of 60-65 m (a.s.l.)) and 209 ky for Aletreika section (at an elevation of 140-145 m (a.s.l.)). The sampling sites are located north of Pineios fault zone and placed on the same fault block, as no trace of interruption of tectonic origin is found between them (Fig. 1).

According to several publications about the sea level fluctuations since Pleistocene the ages of the dated samples belong to the oxygen isotope stages 5.3, 5.5 and 7.3 respectively (Shackleton et al., 1984; Imbrie et al., 1984; Waelbroeck et al., 2002 and references therein). These stages represent high sea level stands for the Mediterranean Sea (Caputo, 2007) and especially for the western coast of Peloponnese (Athanassas and Fountoulis, 2013). Consequently, the contemporary sea level is quite similar to the one during the deposition of the Tyrrhenian strata. In particular, during 103 ka the sea level was at about -13m (a.s.l.), during 118 ka it was at about -1m (a.s.l.) and finally during 209 ka it was at about -7m (a.s.l.) (Waelbroeck et al., 2002).

Taking into account the age of each sample, the sea level changes since Pleistocene and the present elevation of the sampling sections, the uplift rates for the footwall of the Pineios fault zone were calculated approximately at 0.26 mm/yr for Psari area, 0.50 mm/yr for Neapoli area and 0.64 mm/yr for Aletreika area respectively (Fountoulis et al., 2011; 2013). It can be deduced that the maximum uplift rate (0.64 mm/yr) corresponds to an area (Aletreika) located in close proximity to the fault zone in contrast to the other areas which are located much further away to the north (Fig. 1). The differential uplift of the same fault block, containing all three locations, implies a back tilting towards north. The latter in full agreement with the general rotational block faulting mode of structural evolution observed during fieldwork in the surrounding area.

The uplift rate for the hanging wall was also approximately estimated at 0.16 mm/yr (209 ky at the present elevation of 40 m (a.s.l.), which is the lowest elevation on the hanging wall that the same Tyrrhenian layers are cropping out), after considering the sea level during the deposition. It is rather clear that the uplift rate of the hanging wall (0.16 mm/yr) is much lower even than the lowest value of the footwall uplift rate (0.26 mm/yr). The difference between the uplift rate of Aletreika (footwall) and the Pineios River plain (hanging wall) is about 0.48 mm/yr, which corresponds to the actual slip rate of Pineios fault zone for the last 209 ka. This leads to the conclusion that the overall throw of the fault is about 100 meters.

5. GEOELECTRICAL INVESTIGATION

A geophysical survey was carried out at the area of Pineios river valley, downstream of the artificial dam aiming to investigate the layer boundaries between (i) the Holocene fluvial deposits with any other layer covered by them, (ii) the Upper Pleistocene sandstones with the older conglomeratic layer and (iii) the Pleistocene conglomerates with the Pliocene lagoonal marls, since this is the general layer succession described for the broader area (Kamberis et al., 1993). A grid of Vertical Electrical Soundings (VES) was planned around the area distributed on both blocks as the existence of a fault zone underneath the Holocene deposits was quite possible. Vertical Electrical Soundings have been applied successfully for the investigation of geological-tectonic structure in other areas (Alexopoulos and Dilalos, 2010; Alexopoulos et al., 2001; Papadopoulos et al, 2007; Asfahani and Radwan, 2007), sometimes combined also with morphotectonic survey (Asfahani et al., 2010). The geoelectrical data acquisition included two "in-situ" resistivity measurements on surface outcrops of the geological formations and thirteen vertical electrical soundings for the investigation of the geological structure of the area and the possible existence of a fault line at the northern sides of the Pineios riverbed (see Fig. 1 for VES site locations or the supplementary kmz file).

5.1 Geophysical-geological calibration

In order to calibrate and better evaluate the geoelectrical results, the "in-situ" resistivity measurements were carried out (A3 and M1), above known outcrops of the existing geological formations. More specifically the selected sites were located above marls (A3) and sands-sandstones (M1), applying the Schlumberger array, with maximum AB length equal to 430 meters (Fig. 5). This technique contributed to a restrict definition of the corresponding resistivity limits of the most important geological formations of the area and especially for the Plio-Pleistocene lagoonal marls (Table 3). The interpretation results revealed resistivity values of approximately 20 - 25 Ohm.m for the marly layer and 57 - 60 Ohm.m for the Pleistocene Sand, Sandstones and Conglomerates. Moreover, the measured resistivity for the alluvium layers revealed values between 9 - 17 Ohm.m.

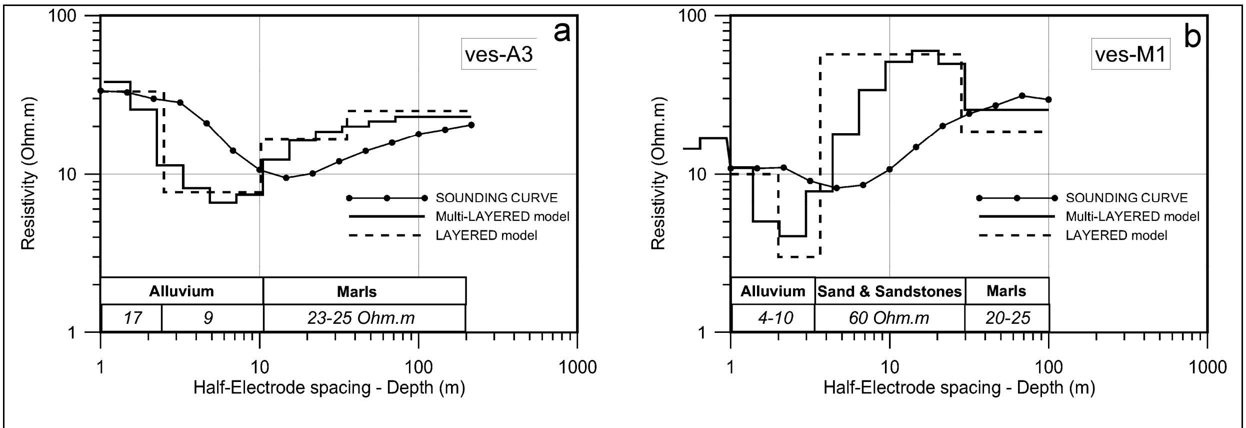

Figure 5. Indicative interpretation results for VES A3 (a) and M1 (b) where several layers were

detected.

Table 3. Resistivity values after the “in situ” geoelectrical measurements.

Geological Formation	Resistivity (Ohm.m)
Upper Pliocene-Pleistocene marls (PlsPt.l)	20 – 25
Sands & Sandstones (Pt.s)	57 – 60

5.2 Acquisition and processing of geophysical data

The Schlumberger array configuration was used for the conduction of thirteen resistivity soundings, in order to investigate the stratigraphic structure of the subsurface geological formations, underlying the study area. The maximum current electrode spacing (AB) reached up to 1,632 meters for most of the measuring sites, which were distributed along three sections with various directions, aiming to cross perpendicular the morphological discontinuity developed north of Pineios river valley. Several kinds of difficulties were met during the current electrode spreading operation, mainly due to the occasionally steep relief, the residual riverbed but also due to local water pits existence and district constructions (streets, fences, etc.). The equipment used for the field measurements included an ABEM Terrameter SAS300C and a Booster 2000.

The acquired geophysical data were processed by applying the automatic method of Zohdy (1989), composing a “multilayer” model. Beyond this, the commercial software package IX1D (v.3.5) of Interpex, was used in order to come up with the “layered” model. In almost all soundings, a formation with resistivity values between 20-28 Ohm.m was detected as the geoelectrical basement (deepest formation), which was evaluated as the Upper Pliocene-Pleistocene marls, based on the “in-situ” measurements.

In order to investigate the lateral inhomogeneity of the geological formations in two dimensions, a distributed apparent resistivity section was created (Fig. 6). This kind of sections, based on the processing of original field data without the intervention of processing algorithms, are often used to provide the quantitative results, which illustrate the complexity of the stratigraphic structure. A first representation is combined and the criteria for the reliability of the applied 1-D geoelectrical soundings are being set. After the qualitative representation and the adumbration of the subsurface general structure, two more sections of distributed (true) resistivity were created, based on results of the multi-layered models using the method described by Zohdy (1989), including the topographic relief into the processing. Furthermore, the layered sections were created according to the results of the 1-D processing and led to the calculated geoelectrical models. Afterwards, all the calculated thicknesses of the geoelectrical layers had been placed at absolute elevations and the subsurface structure illustrated by the geoelectrical layers was reveals for each section. The most significant observation was a clearly defined lateral discontinuity at a distance of about 2,900 meters, at Section C, whilst at Section A, another lateral geoelectrical discontinuity seems to be present at about 750 meters (Fig. 6). Beyond this, the other geoelectrical structure seems to be homogeneously layered with the apparent resistivity values decreasing in depth.

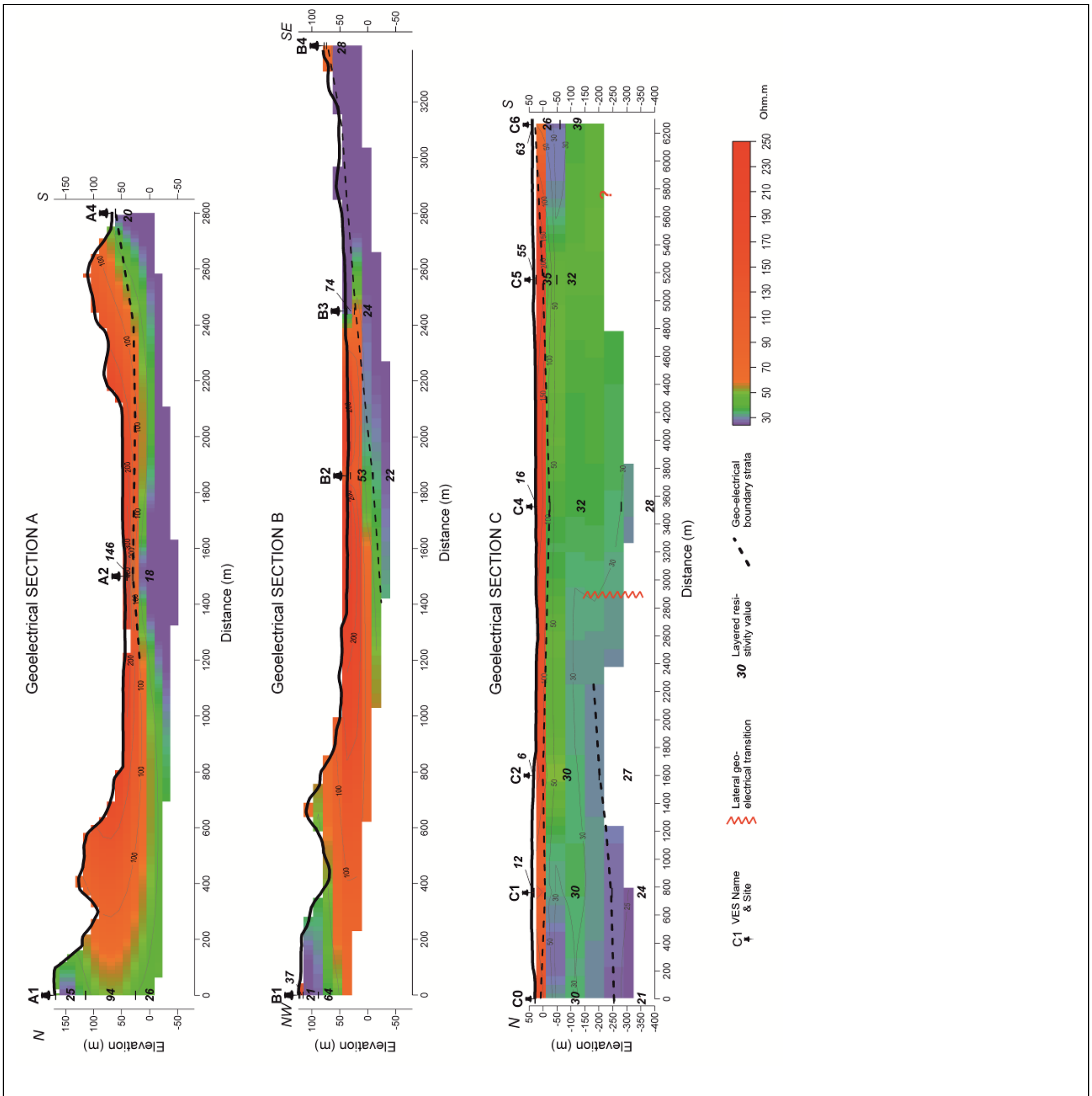

Figure 6. Distribution of resistivity at Sections A, B and C (scale 1:2).

5.4 Geophysical – Geological Conclusions

The geophysical data acquired from the study area were combined with the surface geological observations and the "SOSTI" borehole stratigraphic column by Kamberis et al (1993). The result was the compilation of three geoelectrical-geological sections (Fig. 7) crossing almost perpendicular the Pineios River valley at various directions.

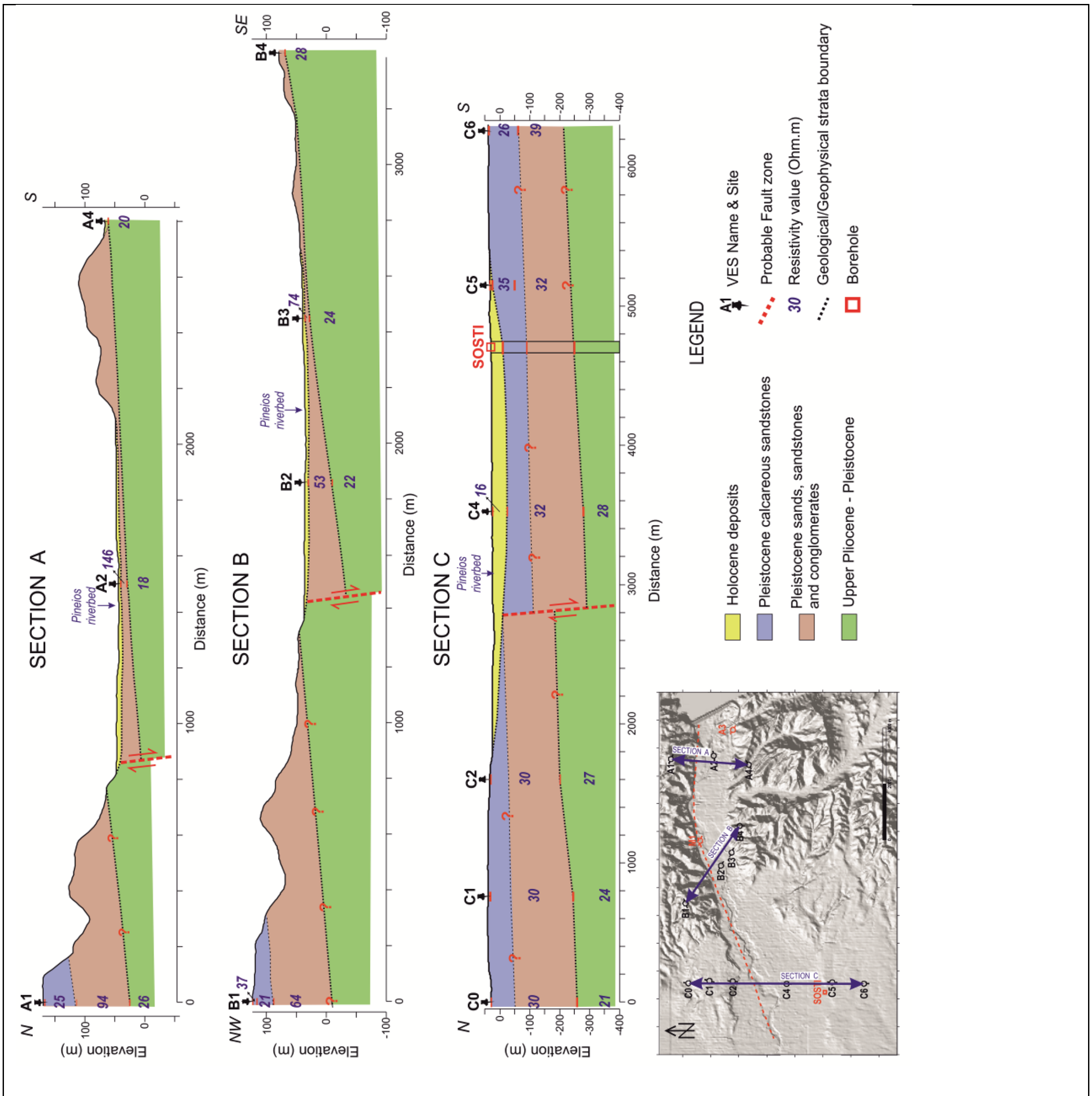

Figure 7. Geological interpretation of the geophysical sections presented at Figure 6 (scale 1:2). The topography is illustrated at the inset map. See figure 1 for the site location distribution.

At these sections the boundaries between four different geological formations have been observed, one of which is the geoelectrical basement of the Upper Pliocene-Pleistocene marls with resistivity values of 20-28 Ohm.m, dipping 10^{o} towards NW, which is in agreement with the surface bedding measurements (Mavroulis, 2009). The Pleistocene sands, sandstones and conglomerates formation (>40 Ohm.m) with a constant thickness of about 100 meters has also been identified overlain the marls, at every section. The Pleistocene calcareous sandstones seem to appear at the highest elevations of the northernmost parts of the three sections as well as south of Pineios riverbed at Section C. It is worth to mention that the resistivity contrast between the latter two formations was quite low and there were objective difficulties for them to be distinguished, but they were overcome due to the detailed and accurate field observations along the morphological discontinuity north of the Pineios River depression.

The interpretation of the geophysical sections yielded the lateral discontinuity to a normal fault zone which is clearly delineated by the interruption of the subsurface layer sequence (Fig. 6, 7) and that is considered to be the major success of the geophysical survey. The fault displacement, based on the top surface of the Plio-Pleistocene marls, is growing from east (~60m at Section A) to west (~110m at Section C) and that is in full agreement with all the surface geological data presented in this study. The uppermost layer of Holocene deposits show an increasing thickness from east (approx. 10m) to west (approx. 60m), which is also in agreement with the increasing down throwing of the fault zone along the same direction.

6. REMOTE SENSING DATA AND SHORELINE DISPLACEMENT ANALYSIS

The main valley that hosts Pineios River runs almost parallel to the fault zone towards west and this happens with no interruption for the last 100 kyr, whatsoever (Raphael, 1973). It is the southward bending downstream that has been changed for the last 2000 years (Kontopoulos and Koutsios, 2010). We argue that its main valley used to flow into the sea by bending northwards somewhere between Markopoulo and Vartholomio (Fig.1). This dramatic change should have a great impact on both the shorelines where the river used to flow into the open sea (Kyllini Bay) and its current estuary to the Ionian Sea. The sediment transportation to both the deltaic areas has been altered during a quite small transition period and the implications on the coastline must have been very significant, especially at such relatively low relief estuary areas. The response of the shoreline in similar cases is always a strong indicator about the sediment transportation change.

Kraft et al., (2005) refer to the existence of the Roman period shoreline several hundreds of meters offshore the Kyllini Bay and this is in agreement with the initial working hypothesis of this study. We argue that the northern coast is under severe erosion and keeps retrograding since the southwards diversion of Pineios River, which have happened around the 5th century (Kontopoulos and Koutsios, 2010). On the contrary on both sides of the new mouth of the river to the south, we expected coastal progradation as the amount of the transported sediment should have increased, at least till the late 1960's when the dam upstream started operating.

6.1 Data acquisition and preparation

We used several remote sensing datasets and topographic maps in order to determine whether or not progradation or retrogradation took place in Pineios former and current deltas during the recent years. We traced the shorelines at different times in a 40-year-period from early 1970's to 2011 using (a) photogrammetrically constructed topographic maps at 1:5,000 scale (1972), (b) two datasets of aerial photos (1987, 1996), and (c) a Landsat-ETM+ satellite image (1999). The traced coastlines were compared to the present shoreline (2011), which was traced with the use of high accuracy Real-Time Kinematics differential GPS (RTK-GPS).

Initially we collected the available data and created a quite satisfactory time series of images along the contemporary coastline. The oldest data available were several sheets of topographic maps acquired from HMGA and their construction was also based on photogrammetry techniques on previously acquired aerial photographs. We used 42 overlapping air photographs, which had been acquired during 1987 and generated an ortho-photo mosaic for this year. During this photogrammetric procedure a high resolution (2-meters) Digital Elevation Model was also produced and used afterwards for the ortho-rectification of a 15-meter resolution Landsat-7 ETM+, panchromatic image, which was acquired during 1999. All the data were co-registered with a 1-meter spatial resolution ortho-photo mosaic created from the photogrammetric interpretation of aerial photographs acquired during 1996 (Fig. 8).

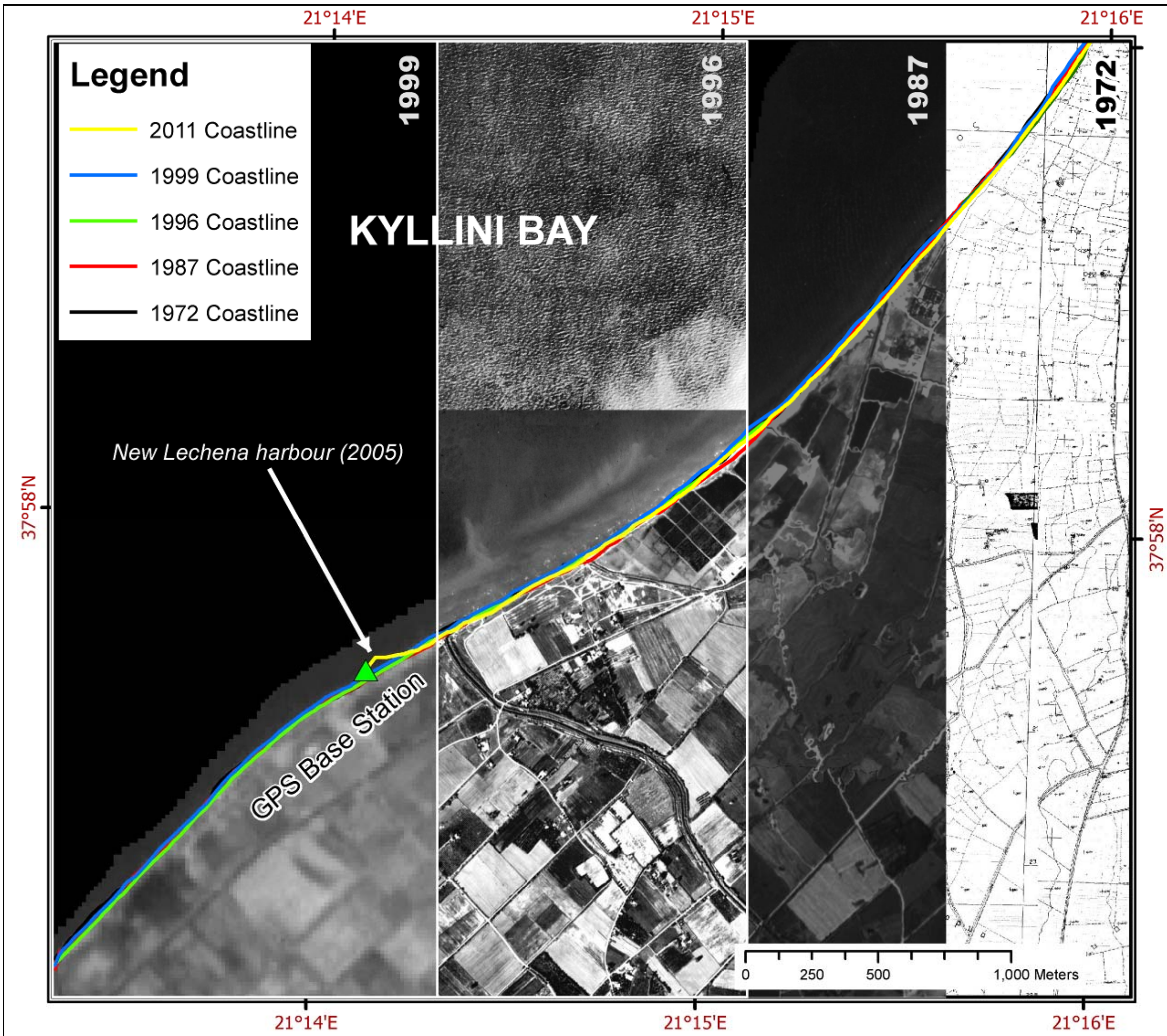

Figure 8. Compilation of the four different types of datasets that were used to trace the historical shorelines. The accuracy varies from 2 to 15 meters depending on the spatial resolution of the data.

The image time series included mainly panchromatic data and therefore the digital products were 8-bit gray-scale images covering most of the study area. By using digital image interpretation techniques we traced the coastline in those different periods. The greater challenge was to identify the exact places of contact between the seawater body and the onshore landscape and consequently increase the accuracy of the measurements. This was made by equalizing the image histogram and in some cases applying a threshold value, which was different at every air-photograph, depending on the orientation of the sunlight. The use of the visible portion of the electromagnetic spectrum for all the collected remote sensing data provides the homogeneity and objectivity of the methodology.

The data acquisition was completed with topographic survey by using the technology of RTK-GPS point collection, after establishing four GPS bases along the shore (Fig. 1). The first three of them were established along the northern coast of the area, covering most of the coast where Pineios River used to flow in the sea. The fourth station was established at the contemporary mouth of Pineios at the southern coast. The rover antenna was setup for acquiring easting and northing coordinates in the Hellenic Geodetic Reference System of 1987 (Greek Grid) projection system, every 50 cm along the shoreline. The accuracy of the present coastline trace was quite high as the specifications of the equipment (TOPCON HiperPro) claim to get measurements with precision less than 10mm. The rover antenna was carried either by walking or adjusted on vehicles driven next to the shoreline where possible. At each case the height of the antenna was measured and imported into the solution software provided by the manufacturer of the equipment (TOPCON Tools v.7).

6.2 Digital shoreline analysis results

The collected points were converted into polylines and projected in a Geographic Information System platform along with the digitized shorelines of the previous years. The best-case scenario would be to have in our disposal five different shorelines for every place but there were smaller or bigger gaps in each datasets due to lack of information or objective difficulty to discriminate the land from the water body during the image interpretation. The combination of all the traced historical coastlines on the remote sensing data with the RTK-GPS recorded coastline have shown that both the former and the current delta fronts of Pineios River are divided into various sub-areas characterized by different type, phase and rate of shoreline displacement.

We used the Digital Shoreline Analysis System (DSAS) version 4.2, which is a software extension to ESRI ArcGIS v.9.3.x published by USGS (Thieler et al., 2009). This extension allows the user to create several transects perpendicular to a baseline parallel to the contemporary shoreline at a given distance and measure the relative position of any digitized coasts. These measurements can be used for extracting the rates of change among other useful statistics. We defined the transect distance every 100 meters along both the north and south coasts and the transect length was 300 meters. A point is automatically created when each transect intersects with the digitized shorelines and its distance to the given baseline is measured. A table of statistics containing all the measured distances is generated after this procedure. We used the statistics focusing along the coastal segments where we had more than four measurements at each transect.

Therefore throughout the total length of 30km of the northern shoreline we used a 13 km segment, which is quite representative for the northern coast. The results show that this part of the coast can be divided in three individual areas. The middle part shows a certain pattern of coastal change, which is strongly affected by a small but significant port (Lechena) which was constructed a few years (harbor works completed during 2005) before the last RTK-GPS measurement (2011). The other two areas seem to have the same behavior, which is retrograding with similar rates. In these cases the eroding rate for the NE part of Kyllini Bay coast is calculated at 0.52 m/yr (Fig. 9a) whilst the SW part is calculated at 0.38 m/yr (Fig. 9b), which are rather compatible. Both of these rates are consistent with the published studies (Raphael, 1973; Kraft et al., 2005) that define the historic shoreline during the late Roman period (~1,550 years BP) several hundreds of meters offshore the contemporary coast and during the Ottoman period (~400 years BP) somewhere in between. With our interpretation the submerged Roman shoreline should have been located 700±250 meters towards NW and the Ottoman shoreline should have been located 190±20 meters at the same direction, more or less parallel to the present one.

At the southern coastal area no significant human impact has been observed for the last century. Therefore the 6.5 km of RTK-GPS measurements are quite satisfactory, although due to lack of remote sensing data we were able to correlate only three shorelines (1972, 1996, 2011) and this was made possible only for 1km, which is rather decent for such a homogenous geo-environment. The aforementioned calculation cannot stand by itself as this area is not very large but it can contribute to this study as a supplementary fact. The rate of the coastal erosion is computed at 0.45 m/yr (Fig. 9c) and this value is also compatible with the results computed for the northern coast even if it was expected to be prograding due to the increase of sediment transportation since the estuary of Pineios River was relocated. A reasonable explanation is that the amount of expected sediment did not reach the river's current mouth at least after the dam construction upstream. The latter is in full operation since 1968 keeping large amounts of eroded materials from reaching the contemporary deltaic area and the oldest shoreline used for this calculation was traced on 1972 topographic maps. Therefore, any prograding influence on the present estuary should have been dramatically reduced after the dam's operation and consequently the coastal erosion prevails.

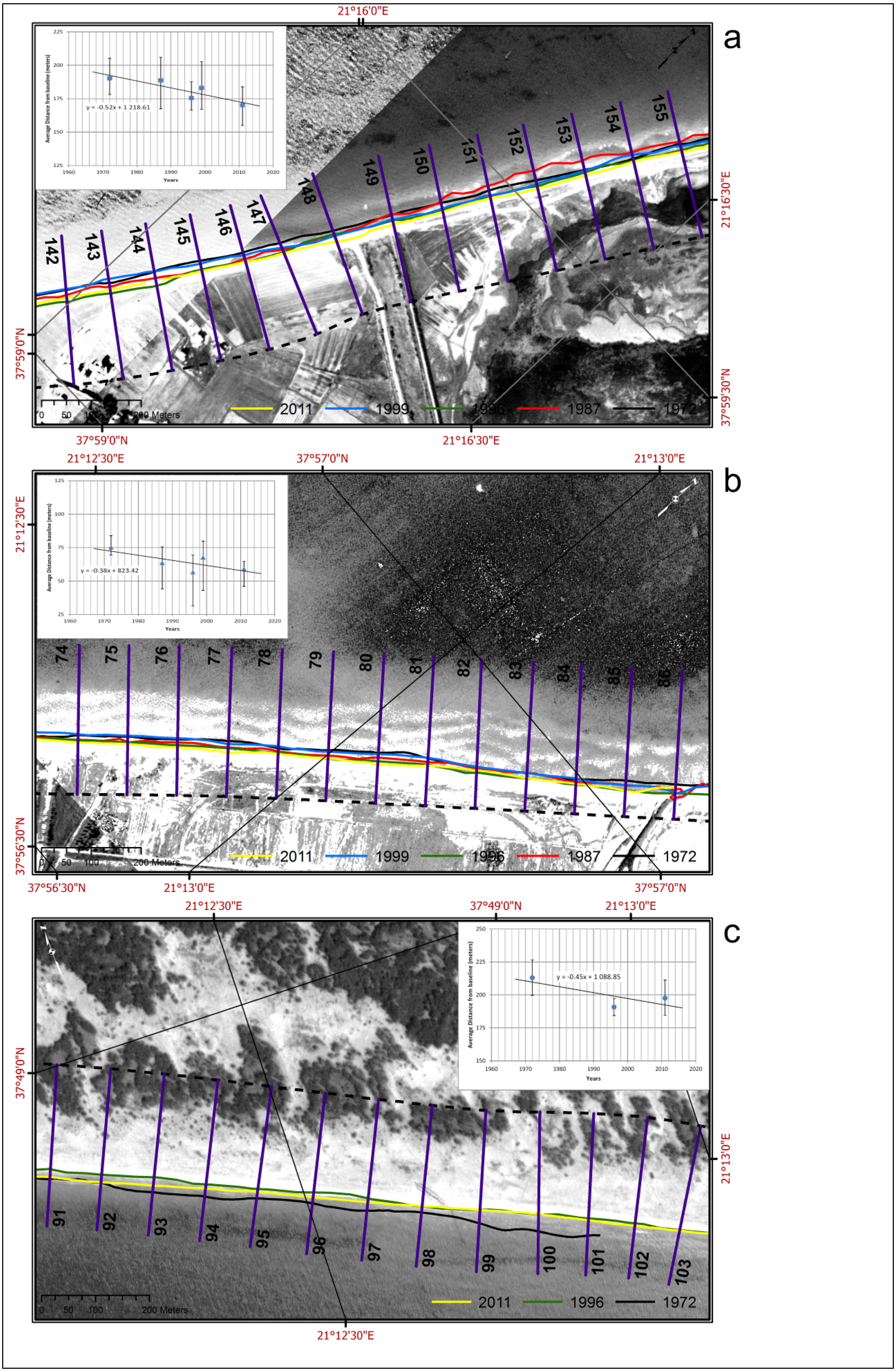
a
b
c
21°16'0"E
21°16'30"E
37°59'0"N
37°59'30"N
y = -0.52x + 1 218.61
Average Distance from baseline (meters)
Years
142
143
144
145
146
147
148
149
150
151
152
153
154
155
2011
1999
1996
1987
1972
21°12'30"E
21°13'0"E
37°57'0"N
37°56'30"N
y = -0.38x + 823.42
74
75
76
77
78
79
80
81
82
83
84
85
86
37°49'0"N
y = -0.45x + 1 088.85
91
92
93
94
95
96
97
98
99
100
101
102
103
200 Meters

Figure 9. Three of the most representative parts of the northern (a,b) and the southern (c) coast, where transects every 100 meters were used for measuring the rates of coastal change. The insets show the trend of the rate of erosion as a result from measuring the horizontal distance from a baseline.

It has to be noted that in this approach, it is assumed that every process that contributes to long-term shoreline changes such as the effect of sea-level rise are included in the historical rate and remains more or less constant over the time frame of 40 years.

7. CONCLUSIONS

We combined several methodologies and different kinds of data to prove that there is an unmapped active normal fault zone trending E-W, crosscutting the area where the artificial lake of Pineios dam is situated.

The geophysical survey verified in depth this tectonic discontinuity between the deposited post-alpine strata by measuring the resistivity gradation along three sections perpendicular to the south dipping normal fault zone. The interpretation of the geophysical measurements revealed that the fault throw is significantly larger at the westernmost segment of the zone, reaching approximately the order of 110 meters. This is in full agreement with the fault slip rate which has been calculated by the differential uplift rates for both of the displaced fault blocks that have been participating in this local tectonic deformation and reaches the order of 0.48 mm/yr for the last 209 ka.

The continuous N-S extensional activity of Pineios fault zone for more than 200ky is causing the relative uplift of the northernmost area and consequently the subsidence of the southernmost block, along with block rotations towards north. The major impact on the river flow is the migration of the location of its estuary, which has been relocated from the northern uplifting fault block to the southern subsiding one. The implications of this relocation are rather obvious on the shorelines and especially along Kyllini Bay (north) where references for submerged ancient coastlines have been noted. The retrograding rate of this shoreline, which is part of the uplifting fault block, is of the order of 0.52 m/yr, since sediment material transportation through Pineios River has been suspended.

Acknowledgments

The author Professor Ioannis Fountoulis passed away (16/2/2013) before the publication of this article. He was a great teacher and a dear friend who left too soon. He will always be an inspiration to us and immeasurably missed. The authors would like to express their appreciation to Dr. V. Mouslopoulou and the two anonymous reviewers whose suggestions and constructive comments highly improved the structure and the maturity of the manuscript. The geophysical survey was funded by Special Account for Research Grants of the UoA (contracts No. 70/4/7620 & 70/4/11078).

REFERENCES

Alexopoulos, J.D., Dilalos S., 2010. Geophysical research for geological structure determination in the region of South Mesogheia (Attica). Bulletin of the Geological Society of Greece, XLIIII(4), 1898-1906.

Alexopoulos, J.D., Fountoulis, I., Kampouris, P., Mariolakos, I., Papadopoulos, T., 2001. Geoelectrical survey for Tatoi (Athens, Greece) blind fault. Bulletin of the Geological Society of Greece, XXXIV(1), 121-127

Asfahani, J., Radwan, Y., 2007. Tectonic Evolution and Hydrogeological Characteristics of the Khanaser Valley, Northern Syria, Derived from the Interpretation of Vertical Electrical Soundings. Pure and Applied Geophysics, 164(11), 2291-2311.

Asfahani, J., Radwan, Y., Layyous, I., 2010. Integrated Geophysical and Morphotectonic Survey of the Impact of Ghab Extensional Tectonics on the Qastoon Dam, Northwestern Syria. Pure and Applied Geophysics, 167(3), 323-338.

Athanassas, C., Fountoulis, I., 2013. Quaternary neotectonic configuration of the southwestern Peloponnese, Greece, based on luminescence ages of marine terraces. Journal of Earth Science, 24(3), 410-427.

Athanassiou, A., 2000. Presence of fossil elephants in the area of Peniós valley (NW Peloponnesus, Greece). Annales Géologiques des Pays Helléniques, 38 (C), 63-76.

Brice, J.C., 1964. Channel patterns and terraces of the Loup Rivers in Nebraska, U.S. Geological Survey Professional Paper, 422-D, Washington.

Bridge, J.S., 2005. Rivers and Floodplains – Forms, Processes, and Sedimentary Record. Blackwell, Oxford.

Bull, W.B., McFadden, L.D., 1977. Tectonic geomorphology north and south of the Garlock fault, California. Geomorphology in arid regions. Proc. 8th Binghamton symposium in geomorphology, 115-138.

Bull, W.B., 1978. Geomorphic tectonic activity classes of the south front of the San Gabriel Mountains, Caliiornia. U.S. Geological Survey Contract Report 14-08-001-G-394, 59.

Caputo, R., 2007. Sea-level curves: Perplexities of an end-user in morphotectonic applications. Global and Planetary Change, 57(3–4), 417-423.

Cotton, C.A., 1950. Tectonic scarps and fault valleys. Geological Society of America Bulletin, 61(7), 717-758.

Cox, R.T., 1994. Analysis of drainage basin symmetry as a rapid technique to identify areas of possible Quaternary tilt-block tectonics: an example from the Mississippi Embayment. Geological Society of America Bulletin, 106, 571-581.

DePolo, C.M., Anderson, J.G., 2000. Estimating the slip rates of normal faults in the Great Basin, USA. Basin Research, 12(3-4), 227-240.

Feng, L., Newman, A.V., Farmer, G.T., Psimoulis, P., Stiros, S.C., 2010. Energetic rupture, coseismic and post-seismic response of the 2008 MW 6.4 Achaia-Elia Earthquake in northwestern

Peloponnese, Greece: an indicator of an immature transform fault zone. Geophysical Journal International, 183(1), 103-110.

Fountoulis, I., Mavroulis, S., Theocharis, D., 2007. Morphotectonic analysis and morphometric indices application in the Lefkochori – Ochthia area (Central-western Peloponnese, Greece), 8th Panhellenic Congress of the Geographical Society of Greece, Athens, Greece, pp. 204-214.

Fountoulis, I., Mavroulis, S., Vassilakis, E., Papadopoulou-Vrynioti, K., 2013. Shoreline displacement and Pineios River diversions in NW Peloponnese (Greece) as result of the geology, active tectonics and human activity during the last 100 ky. Zeitschrift fur Geomorphologie, Supplementary Issues, 57(3), 97-123.

Fountoulis, I., Vassilakis, E., Mavroulis, S., Alexopoulos, J., Erkeki, A., 2011. Quantification of river valley major diversion impact at Kyllini coastal area (W. Peloponnesus, Greece) with remote sensing techniques. In: C. Grützner, T. Fernández Steeger, I. Papanikolaou, K. Reicherter, P.G. Silva, R. Pérez-López, A. Vött (Eds.), 2nd INQUA-IGCP-567 International Workshop on Active Tectonics, Earthquake Geology, Archaeology and Engineering, Corinth, pp. 46-49.

Garrote, J., Cox, R.T., Swann, C., Ellis, M., 2006. Tectonic geomorphology of the southeastern Mississippi Embayment in northern Mississippi, USA. Geological Society of America Bulletin, 118(9-10), 1160-1170.

Guidoboni, E., Comastri, A., Traina, G., 1994. Catalogue of Ancient Earthquakes in the Mediterranean Area up to the 10th Century. Ist. Naz. Geofis., Roma.

Hatzfeld, D., Pedotti, G., Hatzidimitriou, P., Makropoulos, K., 1990. The strain pattern in the western Hellenic arc deduced from a microearthquake survey. Geophysical Journal International, 101(1), 181-202.

Holbrook, J.M., Schumm, S.A., 1998. Geomorphic and sedimentary response of rivers to tectonic deformation: a brief review and critique of a tool for recognizing subtle epeirogenic deformation in modern and ancient settings. Tectonophysics(305), 287-306.

Hollenstein, C., Geiger, A., Kahle, H.G., Veis, G., 2006. CGPS time-series and trajectories of crustal motion along the West Hellenic Arc. Geophysical Journal International, 164(1), 182-191.

Imbrie, J., Hays, J.D., Martinson, D.G., A, M., Mix, A.C., Morley, J.J., Pisias, N.G., Prell, W.L., Shackleton, N.J., 1984. The orbital theory of Pleistocene climate: support from a revised chronology of the marine δ18 O record. In: A. Berger, J. Imbrie, J. Hays, G. Kukla, B. Saltzman (Eds.), Milankovitch and Climate. Reidel, Dordrecht, pp. 269-305

Kamberis, E., 1987. Geology and petroleum geology study of NW Peloponnese, Greece, PhD Thesis, National Technical University of Athens, Athens, Greece.

Kamberis, E., Alexiades, X., Philipe, G., Tsaila-Monopoli, S., Ioakim, X., Tsapralis, B., 1993. Geological Map of Greece, scale 1: 50,000 IGME Athens, pp. Amalias sheet.

Keller, E.A., Pinter, N., 1996. Active Tectonics - Earthquakes, Uplift and Landscape. Prentice Hall, New Jersey.

Konstantinou, K.I., Melis, N.S., Lee, S.-J., Evangelidis, C.P., Boukouras, K., 2009. Rupture Process and Aftershocks Relocation of the 8 June 2008 Mw 6.4 Earthquake in Northwest Peloponnese, Western Greece. Bulletin of the Seismological Society of America, 99(6), 3374-3389.

Kontopoulos, N., Koutsios, A., 2010. A late Holocene record of environmental changes from Kotihi lagoon, Elis, Northwest Peloponnesus, Greece. Quaternary International, 225(2), 191-198.

Koukouvelas, I.K., Kokkalas, S., Xypolias, P., 2010. Surface deformation during the Mw 6.4 (8 June 2008) Movri Mountain earthquake in the Peloponnese, and its implications for the seismotectonics of western Greece. International Geology Review, 52(2-3), 249-268.

Kraft, J.C., Rapp, G., Gifford, J.A., Aschenbrenner, S.E., 2005. Coastal change and archaeological settings in Elis. Hesperia, 74. American School of Classical Studies at Athens, Princeton, NJ.

Lekkas, E., Fountoulis, I., Danamos, G., Skourtsos, E., Gouliotis, L., Mavroulis, S., Kostaki, I., 2008. Seismic fractures related to the NW Peloponnesus (SW Greece) earthquake (ML=6,5R 8-6-2008), EERI, Preliminary Scientific Report

Lekkas, E., Papanikolaou, D., Fountoulis, I., 1992. Neotectonic Map of Greece, scale 1:100,000 Dpt of Dynamic, Tectonic, Applied Geology. EPPO, Athens, pp. sheets Pyrgos – Tropaia.

Lekkas, E., Fountoulis, I., Papanikolaou, D., 2000. Intensity Distribution and Neotectonic Macrostructure Pyrgos Earthquake Data (26 March 1993, Greece). Natural Hazards, 21(1), 19-33.

Leopold, L.B., Wolman, M.G., 1957. River channel patterns: braided, meandering and straight, U.S. Geological Survey Professional Paper, 282-B, Washington.

Margaris, B., Athanasopoulos, G.A., Mylonakis, G., Papaioannou, C., , Klimis, N., Theodulidis, N., Savvaidis, A., Efthymiadou, V., Stewart, J.P., 2010. The 8 June 2008 Mw 6.5 Achaia-Elia, Greece earthquake: Source characteristics, ground motions, and ground failure. Earthquake Spectra, 26(2), 399-424.

Mariolakos, I., Lekkas, E., Danamos, G., Logos, E., Fountoulis, I., Adamopoulou, E., 1991. Neotectonic evolution of the Kyllini Peninsula (NW Peloponnese, Greece). Bull. Geol. Soc. Greece, XXV(3), 163-176.

Mariolakos, I., Papanikolaou, D., Lagios, E., 1985. A neotectonic geodynamic model of Peloponnesus based on morphotectonics, repeated gravity measurements and seismicity. Geol. Jb., B50, 3-17.

Mavroulis, S., 2009. Fault activity assessment in NW Peloponnesus – The Andravida Earthquake (08/06/2008) MSc Thesis, National and Kapodistrian University of Athens, 622 pp.

Mavroulis, S., Fountoulis, I., Lekkas, E., 2010. Environmental effects caused by the Andravida (08-06-2008, ML=6.5, NW Peloponnese, Greece) earthquake. In: A. Williams, G. Pinches, C. Chin, T. McMorran, C. Massey (Eds.), Geologically Active: 11th IAEG Congress. Taylor & Francis Group, Auckland, New Zealand, pp. 451-459.

Mavroulis, S.D., Fountoulis, I.G., Skourtsos, E.N., Lekkas, E.L., Papanikolaou, I.D., 2013. Seismic intensity assignments for the 2008 Andravida (NW Peloponnese, Greece) strike-slip event (June 8, Mw=6.4) based on the application of the Environmental Seismic Intensity scale (ESI

2007) and the European Macroseismic scale (EMS-98). Geological structure, active tectonics, earthquake environmental effects and damage pattern. Annals of Geophysics, 56(6), 10.4401/ag-6239.

Menges, C.M., 1990. Late Quaternary fault scarps, mountain-front landforms, and Pliocene-Quaternary segmentation on the range-bounding fault zone, Sangre de Cristo Mountains, New Mexico. In: E. Krinitzsky, D. Slemmons (Eds.), Neotectonics in earthquake evaluation. Geological Society of America Reviews in Engineering Geology, Boulder, Colorado, pp. 131-156.

Ouchi, S., 1985. Response of alluvial rivers to slow active tectonic movement. Geological Society of America Bulletin, 96(4), 504-515.

Papadopoulos, G.A., Karastathis, V., Kontoes, C., Charalampakis, M., Fokaefs, A., Papoutsis, I., 2010. Crustal deformation associated with east Mediterranean strike–slip earthquakes: The 8 June 2008 Movri (NW Peloponnese), Greece, earthquake (Mw6.4). Tectonophysics, 492(1–4), 201-212.

Papadopoulos, T., Goulty, N., Voulgaris, N.S., Alexopoulos, J.D., Fountoulis, I., Kambouris, P.J., Karastathis, V., Peirce, C., Chailas, S., Kassaras, J., Pirli, M., Goumas, G., Lagios, E., 2007. Tectonic Structure of Central-Western Attica (Greece) based on Geophysical Investigations-Preliminary Results. Bulletin of the Geological Society of Greece, XXXX(3), 1207-1218.

Papanikolaou, D., 1984. The three metamorphic belts of the Hellenides; a review and a kinematic interpretation. In: J.E. Dixon, A.H.F. Robertson (Eds.), The geological evolution of the eastern Mediterranean. Geol. Soc. Spec. Publ. Geological Society of London, Oxford, pp. 551-561.

Papanikolaou, D., 1997. The tectonostratigraphic terranes of the Hellenides. Annales Geologiques des Pays Helleniques , 37, 495-514.

Papanikolaou, D., Fountoulis, I., Metaxas, C., 2007. Active faults, deformation rates and Quaternary paleogeography at Kyparissiakos Gulf (SW Greece) deduced from onshore and offshore data. Quaternary International, 171-172, 14-30.

Papazachos, B.C., Papazachou, C.B., 1997. The Earthquakes of Greece. Ziti, Thessaloniki.

Paraskevaidis, I., Symeonidis, N., 1965. Beitrag zur Kenntnis der Stratigraphie des Neogen von West Peloponnes. Annales Géologiques des Pays Helléniques, XVI, 528-544.

Ramírez-Herrera, M.T., 1998. Geomorphic assessment of active tectonics in the Acambay graben, Mexican Volcanic Belt. Earth Surface Processes and Landforms, 23(4), 317-332.

Raphael, C.N., 1973. Late Quaternary Changes in Coastal Elis, Greece. Geographical Review, 63(1), 73-89.

Rockwell, T.K., Keller, E.A., Johnson, D.L., 1984. Tectonic geomorphology of alluvial fans and mountain fronts near Ventura, California. In: M. Morisawa, T.J. Hack (Eds.), Tectonic Geomorphology. State University of New York, Binghamton, pp. 183-207.

Rust, B.R., 1978. A classification of alluvial channel systems. In: A.D. Miall (Ed.), Fluvial Sedimentology, pp. 187-198.

Schumm, S.A., 1963. Sinuosity of Alluvial Rivers on the Great Plains. Geological Society of America Bulletin, 74(9), 1089-1100.

Shackleton, J.C., Andel, T.H.v., Runnels, C.N., 1984. Coastal Paleogeography of the Central and Western Mediterranean during the Last 125,000 Years and Its Archaeological Implications. Journal of Field Archaeology, 11(3), 307-314.

Silva, P.G., Goy, J.L., Zazo, C., Bardají, T., 2003. Fault-generated mountain fronts in southeast Spain: geomorphologic assessment of tectonic and seismic activity. Geomorphology, 50(1–3), 203-225.

Stamatopulos, L., Voltaggio, M., Kontopulos, N., Cinque, A., La Rocca, S., 1988. ^{230}Th/^{238}U dating of corals from Tyrrhenian marine deposits of Varda area (North–western Peloponnesus), Greece. Geogr. Fis. Dinam. Quat. , 11, 99-103.

Symeonidis, N., Therodorou, G., 1986. New locations of fossil Hippopotamus in northwest Peloponnese. Annales Geologiques des Pays Helteniques, XXXIII (1), 51-67.

Thenius, E., 1955. Hippopotamus aus dem Astien von Elis (Peloponnes). Annales Geologiques des Pays Helleniques, VI, 206-212.

Theocharis, D., Fountoulis, I., 2002. Morphometric indices and tectonically active structures: the case of Salamis island, 6th Panhellenic Geographical Congress, Geogr. Soc. Greece, pp. 97-106.

Thieler, E., Himmelstoss, E., Zichichi, J., Ergul, A., 2009. Digital Shoreline Analysis System (DSAS) version 4.0-An ArcGIS extension for calculating shoreline change, U.S. Geological Survey.

Underhill, J.R., 1988. Triassic evaporites and Plio-Quaternary diapirism in western Greece. Journal of the Geological Society, 145(2), 269-282.

Vassilakis, E., Royden, L., Papanikolaou, D., 2011. Kinematic links between subduction along the Hellenic trench and extension in the Gulf of Corinth, Greece: A multidisciplinary analysis. Earth and Planetary Science Letters, 303(1-2), 108-120.

Waelbroeck, C., Labeyrie, L., Michel, E., Duplessy, J.C., McManus, J.F., Lambeck, K., Balbon, E., Labracherie, M., 2002. Sea-level and deep water temperature changes derived from benthic foraminifera isotopic records. Quaternary Science Reviews, 21(1-3), 295-305.

Wallace, R., 1977. Profiles and ages of young fault scarps, north-central Nevada. Geological Society of America Bulletin, 88(9), 1267-1281.

Wells, S.G., Bullard, T.F., Menges, C.M., Drake, P.G., Karas, P.A., Kelson, K.I., Ritter, J.B., Wesling, J.R., 1988. Regional variations in tectonic geomorphology along a segmented convergent plate boundary pacific coast of Costa Rica. Geomorphology, 1(3), 239-265.

Zámolyi, A., Székely, B., Draganits, E., Timár, G., 2010. Neotectonic control on river sinuosity at the western margin of the Little Hungarian Plain. Geomorphology, 122(3–4), 231-243.

Zohdy, A.A.R., 1989. A new method for the automatic interpretation of Schlumberger and Wenner sounding curves. Geophysics, 54(2), 245-253.